ACS APPLIED MATERIALS & INTERFACES

Research Article

www.acsami.org

Photofunctional Surfaces for Quantitative Fluorescence Microscopy: Monitoring the Effects of Photogenerated Reactive Oxygen Species at Single Cell Level with Spatiotemporal Resolution

Linda Stegemann,[†] Klaus C. Schuermann,[‡] Cristian A. Strassert,*[,†] and Hernán E. Grecco*[,‡,§]

[†]Physikalisches Institut and Center for Nanotechnology (CeNTech), Westfälische Wilhelms-Universität Münster, Heisenbergstraße 11, D-48149 Münster, Germany

[‡]Department of Systemic Cell Biology, Max Planck Institute of Molecular Physiology, Otto-Hahn Straße 11, D-44227 Dortmund, Germany

ABSTRACT: Herein, we report on the implementation of photofunctional surfaces for the investigation of cellular responses by means of quantitative fluorescence microscopy. The developed substrates are able to produce reactive oxygen species under the fluorescence microscope upon irradiation with visible light, and the behavior of cells grown on these surfaces can be consequently investigated *in situ* and *in real time*. Moreover, a suitable methodology is presented to simultaneously monitor photo-triggered morphological changes and the associated molecular pathways with spatiotemporal resolution employing time-resolved fluorescence anisotropy at the single cell level. The results showed that morphological changes can be complemented with a quantitative evaluation of the associated molecular signaling cascades for the unambiguous assignment of reactive oxygen species-related photoinduced apoptosis. Indeed, similar phenotypes are associated with different cellular processes. Our methodology facilitates the *in vitro* design and evaluation of photosensitizers for the treatment of cancer and infectious diseases with the aid of functional fluorescence microscopy.

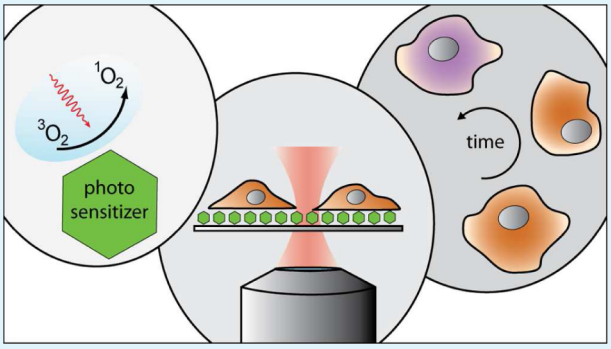

KEYWORDS: *photoactive surfaces, quantitative functional microscopy, reactive oxygen species, cell death, apoptosis, necrosis, caspase activity, phototherapy*

INTRODUCTION

Photodynamic therapy (PDT) is a treatment for multiple diseases, such as cancer and antibiotic-resistant infections, involving the administration (systemically, locally, or topically) of a nontoxic dye known as a photosensitizer (PS). Upon irradiation with visible light, PS molecules generate singlet molecular oxygen ($^1O_2$) by energy transfer from the photo-excited chromphore to triplet molecular oxygen ($^3O_2$). Other reactive oxygen species (ROS) can be also generated by subsequent chemical reactions. This ultimately results in the damage of essential biomolecules, leading to cell death by apoptosis or necrosis.[1,2]

Cellular distribution and concentration of the PS are determinant of the cell fate resulting from the photoinduced damage. It has been shown, for example, that ROS generation in the mitochondria leads to cytochrome c release and formation of the apoptosome complex with apoptotic protease-activating factor-1 (Apaf-1) and recruited procaspase-9. This leads to apoptosis via the cleavage of downstream-effector caspases-3 and -7.[2] In contrast, higher dosages induce necrosis of the irradiated cells, which in turn triggers inflammatory processes in the surrounding tissues. Therefore, it is crucial to find the lowest dose of ROS required to activate the apoptotic pathway, without reaching the threshold that initiates necrotic processes.[3]

The biodistribution of PS in tissues also constitutes a crucial factor that determines the result and effectiveness of a phototherapeutic treatment. Cell-permeating PSs are not necessarily localized in a certain area with particular selectivity but are rather distributed throughout the cell and also in the extracellular medium, leading to unspecific ROS generation.[4] Thus, targeting of tumoral cells is important to attain a selective killing.

Cancerous cells can also be inactivated by triggering immune reactions and by the shutdown of neoplastic neovasculature. Vascular damage indeed poses a significant contribution in the suppression of tumors by withdrawal of nutrients and oxygen through the blood vessels.[5] This reaction is mainly mediated by microvascular stasis, leading to tumoral hypoperfusion and subsequent regression.[6] The pharmacokinetic profile can be influenced by the way of administration of the PS and irradiation progression (drug-light intervals) or by tailoring its

Received: January 8, 2015
Accepted: February 23, 2015
Published: February 23, 2015

DOI: 10.1021/acsami.5b00130
ACS Appl. Mater. Interfaces 2015, 7, 5944−5949

molecular structure. Shorter administration-light intervals primarily affect the vasculature, as the localization of the PS is restricted to the blood vessels. On the other hand, extended drug-light intervals favor cellular damage within the tumor, as the PS effectively permeates into the neoplastic cellular compartments, provided that the sensitizer has a prolonged pharmacokinetic persistence. Such a passive targeting mechanism is mediated by the inherent molecular structure and the derived properties of the PS, such as size, charge, and hydro- and lipophylicity balance.[7] Thus, conjugation of PS with antibodies, nanoparticles, or other macromolecular targeting units unable to permeate across cellular membranes mainly lead to extracellular damage. This is also relevant for the treatment of bacterial infections with highly hydrophilic PS (e.g., polycationic species), as they will be most likely excluded from eukaryotic cells albeit binding to bacteria.

Extracellular PS can also lead to changes in the intracellular milieu. In addition to the described toxicity of ROS, it has recently become evident that certain ROS species such as hydrogen peroxide (H_2O_2) also constitute a class of signaling molecules.[8] Indeed, H_2O_2 not only represents the unwanted yet inevitable byproduct of aerobic metabolism but also mediates diverse physiological responses such as cell proliferation, differentiation, and migration.[9] Moreover, death receptors such as tumor necrosis factor (TNF) are also able to induce ROS via NOX,[2] creating an interplay between apoptotic signaling and cytotoxicity. In particular, reversible oxidative inactivation of diverse protein tyrosine phosphatases (PTP) has been demonstrated upon stimulation with growth factors.[10] Due to its high reactivity, the sphere of $^1O_2$ activity has a radius of ca. 150 nm from its point of production.[11] In this way, a nanoenvironment of low PTP activity could be the mechanism by which high receptor tyrosine kinase (RTK) activity is maintained upon irradiation and extracellular ROS production.[12]

In view of the above-mentioned aspects, it is abundantly clear that a rational development of selective PS requires a detailed understanding of the molecular bases, the dynamics, and the kinetic factors governing the extracellular damage that is inflicted by photoinduced ROS generation, which in turn need to be compared with intracellular photosensitization processes. In this context, the characterization of PS for PDT involves the quantitative understanding of the phototriggered signaling pathways originated by different classes of exposures. Ogilby and co-workers[13] have recently demonstrated the utility of a neutral, highly hydrophilic PS for the confined extracellular production of ROS by confocal irradiation. It was shown that this hydrophilic, membrane-impermeable $^1O_2$ sensitizer induces morphological cellular changes comparable to those described as apoptosis and necrosis. This pioneering work poses the challenge to investigate potential quantitative correlations between morphological criteria and phototriggered molecular reaction pathways.[14] With this background in mind, we herein report on the development of photofunctional surfaces for active fluorescence microscopy involving the spatiotemporally resolved photogeneration of ROS with simultaneous monitoring of the photoinduced morphological changes and the resulting molecular pathways with spatiotemporal resolution at single cell level. In particular, we demonstrate how this can be achieved by growing HeLa cells on microscopy substrates functionalized with poly-L-lysine that has been covalently conjugated with a PS. The morphological changes upon confocal and wide-field irradiation were monitored for the extracellular photoproduction of ROS and compared with the effects of the same membrane-permeating PS freely dissolved in the culture medium. In order to monitor apoptotic molecular cascades, the cells were transfected with a homo-FRET anisotropy caspase-3 sensor based on the work of Harpur et al.[15] Cells treated with staurosporine or without any PS were used as positive and negative controls for caspase-3 activity, respectively. We observed that the localized (confocal irradiation) and wide-field photoproduction of ROS (both at extra- and intracellular level) can originate apoptosis-like morphological changes. Most importantly, the concomitant apoptosis-related caspase activity was reliably monitored by time-resolved fluorescence anisotropy microscopy at single cell level.

EXPERIMENTAL SECTION

Materials. Poly-L-lysine was used for surface coating. Dicarboxymethylene blue (MB) *N*-hydroxysuccinimide (NHS) ester, commercially available at emp Biotech GmbH, was used as a PS for functionalizing glass surfaces. Coverslips functionalized with amino groups (NEXTERION) were purchased from Schott AG.

Fabrication and Characterization of Substrates. Surface functionalization was carried out in a sterile environment and with sterile solvents on clean substrates (glass and NEXTERION coverslips were cleaned with ethanol; sterile LabTek 8-wells chambers were purchased) by coating with a 30 mg/mL solution of poly-L-lysine in PBS, incubating for approximately 30 min and subsequently washing with PBS and ddH_2O. Afterward, a 68 μM solution of MB-NHS ester in PBS was added to the poly-L-lysine-coated substrates, incubated for 30 min, and washed with PBS, water, and ethanol. Both the NEXTERION substrates and poly-L-lysine-coated surfaces showed a slight blue coloring after the reaction, and the functionalization was additionally verified by absorption measurements with a Cary 5000 UV−vis spectrophotometer from Varian.

The coverslips were measured with the aid of a solid state sample holder. The baseline was recorded with two poly-L-lysine-coated coverslips at first, and then, the coverslips functionalized with the PS were measured. Emission spectra of the coverslips were measured in front-face mode with a Fluorolog 3 from Horiba Jobin Yvon. For the emission spectra, the excitation monochromator was set to 590 nm with a slit width of 14 nm. The emission wavelength was scanned from 640 to 800 nm, and the slit was set to 8 nm. The integration time was 0.5 s.

Caspase Biosensor. The caspase-3 sensor[15] comprises two *m*-Citrine fluorophores connected by a cleavage site (DEVD). The two fluorophores are in close proximity and thus undergo homo-FRET, which can be observed by decreased fluorescence anisotropy as compared with the *m*-Citrine monomer. When caspase-3 is active, it cuts the cleavage site and the two fluorophores are separated, thus interrupting the homo-FRET and resulting in an increase in anisotropy.

Cell Culture. Cells were grown in Lab-Tek 8-well chambers each functionalized with poly-L-lysine and PS as described in the previous paragraph. The cells were split and added to the wells in Dulbecco's modified Eagle's medium (DMEM) supplemented with 10% fetal cow serum (FCS). After the cells had a minimum of 12 h to attach to the surface, they were ready for transfection. For transfection, 6 μL of Fugene 6 from Roche was added to 200 μL of serum free DMEM and incubated for 5 min at room temperature. Afterward, 2 μg of the DNA encoding for the caspase-3 homoFRET biosensor was added; the mixture was vortexed and incubated for 15 min at room temperature, after which 25 μL of this mixture was added to each well and the transfected cells were allowed to express by incubating them at 37 °C with 5% CO_2 for at least 20 h. Before the microscopy experiments, the medium was changed to low bicarbonate DMEM without phenol red and supplemented with 25 mM Hepes, pH 7.4 (imaging medium).

Confocal Microscopy. The confocal images were recorded on a Leica SP5 confocal microscope with a 63× oil immersion objective

DOI: 10.1021/acsami.5b00130
ACS Appl. Mater. Interfaces 2015, 7, 5944−5949

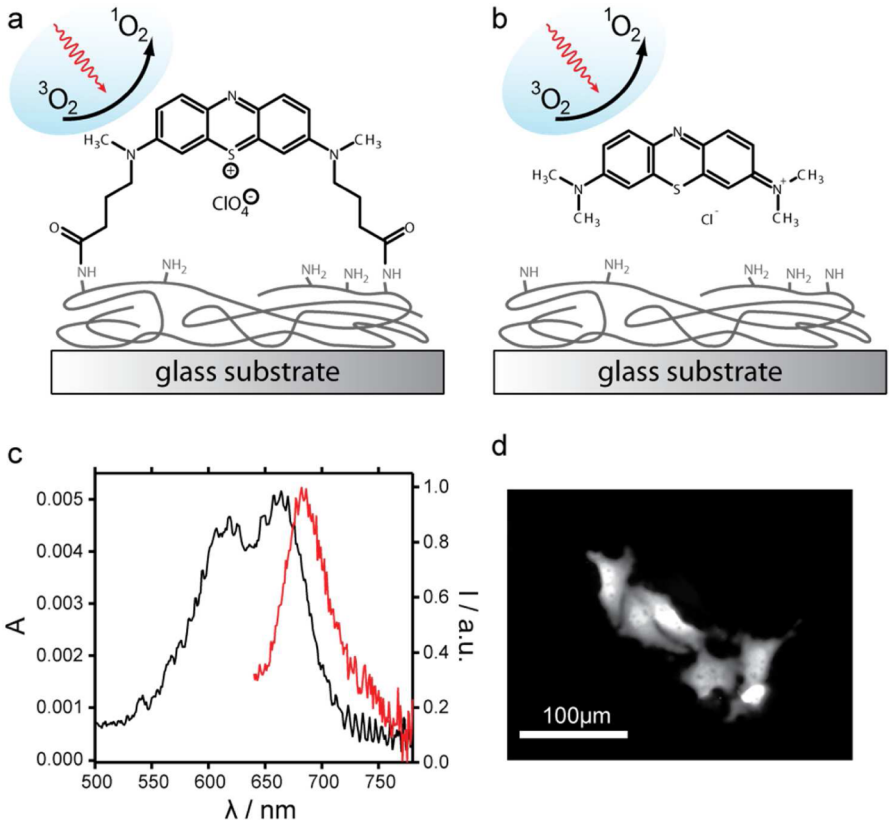

Figure 1. Photoactive surfaces for functional microscopy. (a) Functionalization of poly-L-lysine-coated substrates with MB-NHS ester. (b) Poly-L-lysine coated substrates in combination with freely diffusing MB in solution. (c) Absorption and emission spectrum of (a). (d) HeLa cells grown on (a).

(NA 1.4). The sample was excited by a 488 nm laser (3.0 μW), and emission was observed between 510 and 580 nm. The methylene blue (MB) was excited through the objective by scanning a small ROI repeatedly with a 633 nm laser (94 μW).

Fluorescence Anisotropy Microscopy. The wide-field microscopy images were recorded on an Olympus IX81 inverted microscope (Olympus, Germany) with an MT20 illumination system for excitation. The excitation light was filtered by a YFP excitation filter (490−500 nm), and the emission was measured through a 505 nm dichroic and a 535/30 nm bandpass filter. A linear dichroic polarizer (Meadowlark Optics, Frederick, Colorado, US) was placed in the illumination path of the microscope, and two identical polarizers were placed in an external filter wheel at orientations parallel and perpendicular to the polarization of the excitation light. The fluorescence was collected via a 20×, 0.7 NA air objective, and parallel and perpendicular polarized emission images were acquired sequentially on an Orca CCD camera (Hamamatsu Photonics, Japan). Before each experiment, a dilute solution of fluorescein was measured in order to calculate the G-factor. The activation of MB was performed through the objective using a Cy5 filter set (exc. 628/40 nm dichroic 660 nm) with a light power of 8.0 mW. For each of the conditions, a few positions with multiple cells each were saved and then repeatedly measured in 30 min intervals.

Analysis. The anisotropy images were calculated by

$$r = \frac{I_{\parallel} - GI_{\perp}}{I_{\parallel} + 2GI_{\perp}}$$

where $I_{\parallel}$ and $I_{\perp}$ denote the background-corrected parallel and perpendicular images. The background was estimated from the average intensity in a small ROI outside the cells. The polarizers can introduce a small shift between the two images which is constant throughout the experiment. This was calculated from manually shifting the images until the overlap was perfect for one image set and then applied to all images.

The *G*-factor was calculated from fluorescein solution using

$$G = \frac{I_{\parallel}}{I_{\perp}}$$

The fluorescence images were used to identify cells and create cell masks which were tracked over time. For each identified cell, the average anisotropy and fluorescence intensity were calculated. All image analysis has been performed in CellProfiler.[16]

The above-described method yields a time-trace for each cell which can be further analyzed to identify the cells fate. In case of an activation of the caspase-3 activity, the anisotropy is expected to rise quickly from the anisotropy of double *m*-Citrine to the anisotropy of the free *m*-Citrine. This curve was fitted with a Boltzmann sigmoidal function where the intersection of the slope at the turning point of the sigmoidal curve and the baseline was defined as a point of activation. Cells that showed a higher anisotropy at the beginning of the experiment and thus appeared already dead or dying were filtered out. Cells that showed no significant rise in anisotropy ($\Delta r < 0.03$) were considered alive during the whole experiment.

RESULTS AND DISCUSSION

In order to create a photoactive surface for functional microscopy, we covered the glass bottom of 8-well chambers with poly-L-lysine, a natural coating agent used in cell culture to facilitate cellular adherence onto surfaces, as it provides positive charges that interact electrostatically with the negatively charged membrane moieties of cells. Poly-L-lysine does not bind covalently to the glass surfaces, but its electrostatic adhesion toward the substrate is sufficiently strong to avoid detachment upon addition of growth medium. In order to

DOI: 10.1021/acsami.5b00130
ACS Appl. Mater. Interfaces 2015, 7, 5944−5949

immobilize the PS on the surface, the NHS ester of MB was bound to the free amino groups of poly-L-lysine (Figure 1a). This MB derivative was chosen as it is able to bind covalently to free amino groups, forming stable amide bonds and allowing a straightforward functionalization in aqueous solutions. Moreover, its properties can be easily compared with freely diffusing MB in solution (Figure 1b) possessing a $^1O_2$ quantum yield of 0.52 in water. After the functionalization, the substrates showed a slight blue tint, as confirmed by the absorption and emission spectra (Figure 1c).[17] The maximum of the emission spectrum (663 nm) is slightly blue-shifted (505 cm^{-1}) as compared to the fluorescence maximum given by the commercial supplier (686 nm, in water), which can be attributed to the polar environment of the poly-L-lysine.[18] Most importantly, the functionalization did not affect the cell adhesion onto the substrates (Figure 1d), rendering this strategy as adequate for live cell experiments. It is worth mentioning that the MB-NHS ester was also bound to coverslips functionalized with amino groups (NEXTERION, Schott) as an alternative to the aforementioned protocol. However, cell adhesion was completely hampered in this case. The $^1O_2$ photogenerated by the MB bound to the poly-L-lysine can directly react with cellular structures, e.g., membrane components lying in close contact with the substrate. $^1O_2$ molecules that eventually diffuse away, on the other hand, are physically quenched by water or N−H vibrations of the poly-L-lysine, thus preventing the secondary production of other ROS that could further interact with the cell.

Dividing the absorbance at the absorption maximum (0.0049) by the molar absorption coefficient of MB-NHS (53×10^3 M^{-1} cm^{-1}, i.e., 8.8×10^{-17} molecules cm^3 cm^{-1}), we estimated a surface PS concentration of 5.5×10^{13} molecules/cm^2. Therefore, approximately 8.8×10^8 PS molecules are available for a typical HeLa cell, as it encompasses an area of 10^{-5} cm^2.[19] It should be noted that only a fraction of the short-lived $^1O_2$ can reach the cells growing on the substrate, even though every PS molecule is in principle available for $^1O_2$ production. For comparative purposes, cells grown on poly-L-lysine-coated substrates were also used in combination with freely diffusing MB that had been predissolved in the growth medium. Since part of the ROS generated at the poly-L-lysine-coated surface is lost due to physical quenching by O−H or N−H vibrations, a 30-fold lower number of dissolved MB molecules per cell was employed (2.8×10^7) as compared to surface-immobilized PS. A similar MB concentration (12.5 μM) has been previously used on studies with HeLa cells.[20]

We first looked at the effect of localized $^1O_2$ generation on HeLa cells. In a confocal microscope, we selectively irradiated a specific area of the cell body and then imaged the phenotypic response for 10 min. As expected, a characteristic blebbing was observed for cells treated with the membrane-permeating PS, independently of the subcellular localization of the irradiation (Figure 2a). Moreover, rounding and detaching were observed upon irradiation in the center of the cells along with blebbing of nonirradiated neighboring cells. None of these behaviors were observed without irradiation (data not shown) or when the same irradiation was applied to cells grown on poly-L-lysine-coated substrates but without any PS, indicating that the photogenerated ROS is unambiguously responsible for this observation.

On the other hand, cells growing on MB-functionalized surfaces displayed a significantly different behavior, depending on the location of the irradiation. Upon localized generation of

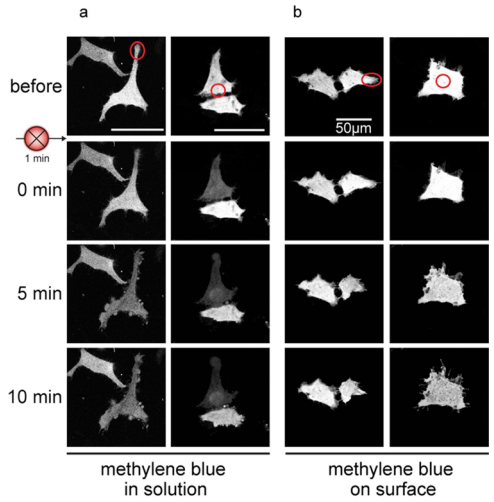

Figure 2. Localized ROS generation. Confocal microscopy of HeLa cells before and after confocal irradiation of a small region (red circles) with a 633 nm HeNe laser with (a) MB in solution or (b) surface-immobilized MB.

$^1O_2$ at the periphery of a cell, blebs were not observed, even though the cells retracted from the irradiated area (Figure 2b, left). Interestingly, the original shape was recovered upon interruption of the excitation with light. In contrast, formation of blebs throughout the entire cell was observed when $^1O_2$ was generated in its center (Figure 2b, right). The lack of blebbing, cell rounding, or detaching upon peripheral confocal irradiation on MB-functionalized surfaces, along with the cell retraction observed instead, lead us to question if the blebbing detected upon confocal irradiation in the center of the cell body was actually related to an apoptotic process for the MB-functionalized surfaces. Cell blebbing is usually taken as a proxy of apoptotic cell death in phototoxicity experiments.

To be independent from the localization of the irradiation, we performed phototoxicity experiments using wide-field illumination to generate $^1O_2$ ubiquitously throughout the cell. Wide-field microscopy also allowed us to measure a larger number of cells in a shorter time. We irradiated the cells for 1 min periodically every 30 min, thereby allowing us not only to quantify the effect of a single light shot as before but also to assess the cumulative dose. We observed phenotypic responses comparable to those monitored upon confocal irradiation of the cell centers: The cells showed blebbing for both the freely diffusing MB (Figure 3a), as well as for the PS linked to the surface (Figure 3b). However, the blebs on the cells with the internalized PS showed a different pattern than for the cells on the photosensitizing surfaces. This hinted again to the fact that a different process might be underlying the phenotypic change on the different substrates.

While blebbing is usually taken as a sign for apoptosis induction, further insights into the actual molecular signaling mechanisms were pursued. HeLa cells were transfected with a homo-FRET anisotropy sensor consisting of two *m*-Citrine molecules with a DEVD-linker that is cleaved upon activation of caspase-3 (Figure 4a). In this case, homo-FRET leads to a loss of fluorescence anisotropy for coupled *m*-Citrine units. When caspases are activated, the linker is cut and homo-FRET is suppressed; the fluorescence anisotropy of individual *m*-Citrine molecules is recovered. Thus, fluorescence anisotropy constitutes a direct measurement of the cumulative activity of

DOI: 10.1021/acsami.5b00130
ACS Appl. Mater. Interfaces 2015, 7, 5944−5949

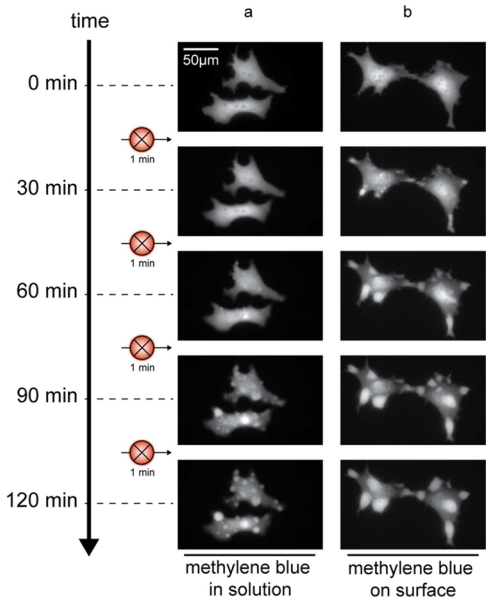

Figure 3. Ubiquitous ROS generation by wide-field irradiation. Fluorescence images of cells with (a) MB in solution or (b) surface-immobilized MB upon 1 min wide-field irradiation every 30 min.

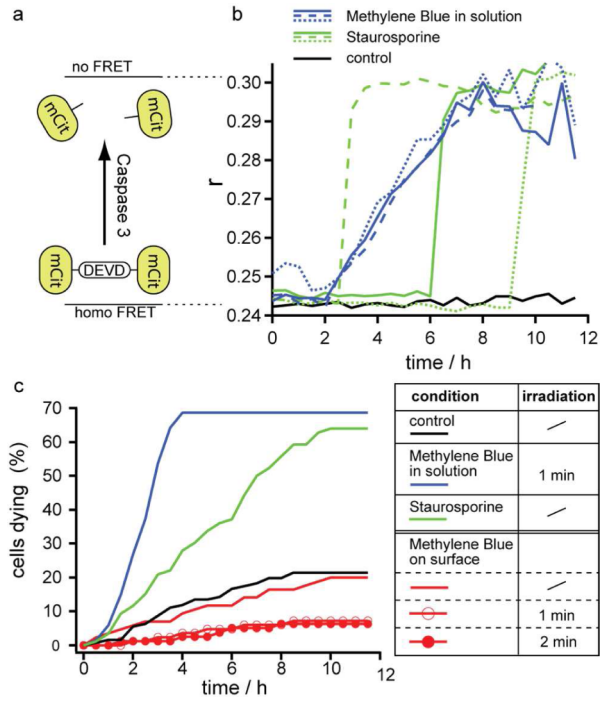

Figure 4. Apoptosis assay and analysis: (a) Scheme of the homo-FRET caspase-3 sensor. (b) Sigmoid activation curves of the sensor upon different stimulations for different individual cells. (c) Fraction of caspase-3 active cells over time, as calculated from (b).

caspase-3, showing a transition from inactive to active in individual cells for different treatments (Figure 4b).

Individual staurosporine-treated cells (Figure 4b, green lines) yielded diverse caspase-3 onsets along with steeper activation profiles than those obtained by irradiation of cells treated with MB in solution (Figure 4b, blue lines). This is most likely due to the fact that staurosporine directly activates caspase-3, whereas the ROS-induced caspase-3 activity is probably due to a cumulative effect. From the individual sigmoid curves (such as those depicted exemplarily in Figure 4b), an activation time was obtained for each cell (for more details, see the Experimental Section) and plotted as the fraction of caspase-3-active cells as a function of time (Figure 4c). Notably, irradiation of cells treated with MB in solution induced an average caspase-3 activation that is faster than for staurosporine-stimulated cells and significantly faster than the controls (without staurosporine and PS). It was interesting to find out that irradiation of cells grown on MB-functionalized surfaces activated caspase-3 significantly slower than the negative control (without any PS and staurosporine). However, this rather surprising finding correlates with the fact that these cells stopped blebbing and recovered once the irradiation was interrupted. We speculate that, due to its short diffusion range, surface-generated ROS predominantly triggers signaling mechanisms that actually protect the cells from apoptosis, rather than inducing it. For example, it has been reported that low doses of H_2O_2 increase the expression of thioredoxin-1, an oxidoreductase with antiapoptotic effects.[21] Similarly, it has been shown that endothelial growth factor receptor-3 signaling in response to H_2O_2 promotes endothelial cell survival.[22] The exact protecting molecular mechanism is an open question for future studies, but it is clear that the observed blebbing reaction does not constitute an apoptotic process but rather a response of the cytoskeleton to the ROS.

CONCLUSIONS AND PERSPECTIVES

In summary, we have shown a straightforward method for the spatiotemporally resolved ROS generation implementable for diverse microscopy techniques. The photofunctional surfaces provide a versatile tool for the external perturbation of living cells in the quantitative investigation of cell dynamics, as poly-L-lysine-coated glass constitutes a suitable substrate for cell adhesion.

In concordance with earlier studies employing nonpermeable PS, we observed retraction and blebbing of the cells upon ROS generation by localized confocal irradiation in a confined cellular region. However, comparison of these observations with the effect of a membrane-permeating PS that was also activated by confocal irradiation pointed toward an essentially different underlying biological mechanism. This was confirmed by wide-field irradiation experiments comparing the freely diffusing and the surface-bound PS and monitoring the temporal evolution of apoptosis-related molecular markers. Using a homo-FRET sensor to monitor caspase activity, we showed that apoptosis was not induced with the surface-bound PS. Actually, the cells were protected from apoptosis upon external ROS generation, despite the apoptosis-like blebbing.

While the detailed underlying mechanisms will be addressed in the future, our results clearly demonstrate that diverse aspects regarding cellular biology can be addressed by the judicious combination of biocompatible photoactive substrates and quantitative microscopy. With these tools, the assessment of the apoptotic or necrotic potential of tailored PS is possible beyond the simple observation of cell morphology or different phenotypes. The evaluation and optimization of new PS is indeed facilitated, as functional microscopy is able to unravel the underlying molecular mechanisms. We envisage that our methodology applied to the *in vitro* evaluation of PS will provide new fundamental insights concerning the phototreatment of cancer and infectious diseases, as functional microscopy provides simultaneous morphological and molecular readouts in real time.

DOI: 10.1021/acsami.5b00130
ACS Appl. Mater. Interfaces 2015, 7, 5944−5949

AUTHOR INFORMATION

Corresponding Authors

*E-mail: ca.s@wwu.de.
*E-mail: hgrecco@df.uba.ar.

Present Address

[§]H.E.G.: Laboratorio de Electrónica Cuántica, Departamento de Física, Facultad de Ciencias Exactas y Naturales, Universidad de Buenos Aires and IFIBA, CONICET, Argentina.

Notes

The authors declare no competing financial interest.

ACKNOWLEDGMENTS

Financial support from the Deutsche Forschungsgemeinschaft (Projects STR1186/1-1 and GR 3848/1-1) is gratefully acknowledged.

REFERENCES

(1) Dolmans, D. E. G. J.; Fukumura, D.; Jain, R. K. Photodynamic Therapy for Cancer. *Nat. Rev. Cancer* **2003**, *3*, 380−387.

(2) Circu, M. L.; Aw, T. Y. Reactive Oxygen Species, Cellular Redox Systems, and Apoptosis. *Free Radic. Biol. Med.* **2010**, *48*, 749−762.

(3) Lavie, G.; Kaplinsky, C.; Toren, A.; Aizman, I.; Meruelo, D.; Mazur, Y.; Mandel, M. A Photodynamic Pathway to Apoptosis and Necrosis Induced by Dimethyl tetrahydroxyhelianthrone and Hypericin in Leukaemic Cells: Possible Relevance to Photodynamic Therapy. *Br. J. Cancer* **1999**, *79*, 423−432.

(4) Castano, A. P.; Demidova, T. N.; Hamblin, M. R. Mechanisms in Photodynamic Therapy: Part One-Photosensitizers, Photochemistry and Cellular Localization. *Photodiagnosis Photodyn. Ther.* **2004**, *1*, 279−293.

(5) Kamarulzaman, E. E.; Benachour, H.; Barberi-Heyob, M.; Frochot, C.; Wahab, H. A.; Guillemin, F.; Vanderesse, R. Vascular-Targeted Photodynamic Therapy (VTP). In *Advances in Cancer Therapy*; Gali-Muhtasib, H., Ed.; In Tech: Rijeka, Croatia, 2011; ISBN: 978-953-307-703-1.

(6) Wang, W.; Moriyama, L. T.; Bagnato, V. S. Photodynamic Therapy Induced Vascular Damage: An Overview of Experimental PDT. *Laser Phys. Lett.* **2013**, *10*, 023001.

(7) Chen, B.; Pogue, B. W.; Hoopes, P. J.; Hasan, T. Vascular and Cellular Targeting for Photodynamic Therapy. *Crit. Rev. Eukaryotic Gene Expression* **2006**, *16*, 279−305.

(8) Rhee, S. H_2O_2, a Necessary Evil for Cell Signaling.G. *Science* **2006**, *312*, 1882−1883.

(9) Rhee, S. G.; Bae, Y. S.; Lee, S.-R.; Kwon, J. Hydrogen Peroxide: A Key Messenger that Modulates Protein Phosphorylation Through Cysteine Oxidation. *Sci. Signaling* **2000**, *2000*, pe1.

(10) Tonks, N. K. Redox Redux: Revisiting PTPs and the Control of Cell Signaling. *Cell* **2005**, *121*, 667−670.

(11) Ogilby, P. R. Singlet Oxygen: There is Indeed Something New under the Sun. *Chem. Soc. Rev.* **2010**, *39*, 3181−3209.

(12) Tischer, C.; Bastiaens, P. I. H. Lateral Phosphorylation Propagation: An Aspect of Feedback Signalling? *Nat. Rev. Mol. Cell Biol.* **2003**, *4*, 971−975.

(13) Pimenta, F. M.; Jensen, R. L.; Holmegaard, L.; Esipova, T. V.; Westberg, M.; Breitenbach, T.; Ogilby, P. R. Singlet-Oxygen-Mediated Cell Death Using Spatially-Localized Two-Photon Excitation of an Extracellular Sensitizer. *J. Phys. Chem. B* **2012**, *116*, 10234−10246.

(14) Klotz, L. O.; Pellieux, C.; Briviba, K.; Pierlot, C.; Aubry, J. M.; Sies, H. Mitogen-Activated Protein Kinase (p38-, JNK-, ERK-) Activation Pattern Induced by Extracellular and Intracellular Singlet Oxygen and UVA. *Eur. J. Biochem.* **1999**, *260*, 917−922.

(15) Harpur, A. G.; Wouters, F. S.; Bastiaens, P. I. H. Imaging FRET Between Spectrally Similar GFP Molecules in Single Cells. *Nat. Biotechnol.* **2001**, *19*, 167−169.

(16) Kamentsky, L.; Jones, T. R.; Fraser, A.; Bray, M.-A.; Logan, D. J.; Madden, K. L.; Ljosa, V.; Rueden, C.; Eliceiri, K. W.; Carpenter, A. E. Improved Structure, Function and Compatibility for CellProfiler: Modular High-Throughput Image Analysis Software. *Bioinformatics* **2011**, *27*, 1179−1180.

(17) Lewis, G. N.; Goldschmid, O.; Magel, T. T.; Bigeleisen, J. Dimeric and Other Forms of Methylene Blue: Absorption and Fluorescence of the Pure Monomer. *J. Am. Chem. Soc.* **1943**, *65*, 1150−1154.

(18) Mirenda, M.; Strassert, C. A.; Dicelio, L. E.; San Román, E. Dye-Polyelectrolyte Layer-by-Layer Self-Assembled Materials: Molecular Aggregation, Structural Stability, and Singlet Oxygen Photogeneration. *ACS Appl. Mater. Interfaces* **2010**, *2*, 1556−1560.

(19) Puck, T. T.; Marcus, P. I.; Cieciura, S. J. Clonal Growth of Mammalian Cells in Vitro; Growth Characteristics of Colonies from Single HeLa Cells with and without a Feeder Layer. *J. Exp. Med.* **1956**, *103*, 273−283.

(20) Stockert, J. C.; Juarranz, A.; Villanueva, A.; Cañete, M. Photodynamic Damage to HeLa Cell Microtubules Induced by Thiazine Dyes. *Cancer Chemother. Pharmacol.* **1996**, *39*, 167−169.

(21) Haendeler, J.; Tischler, V.; Hoffmann, J.; Zeiher, A. M.; Dimmeler, S. Low Doses of Reactive Oxygen Species Protect Endothelial Cells from Apoptosis by Increasing Thioredoxin-1 Expression. *FEBS Lett.* **2004**, *577*, 427−433.

(22) Wang, J. F.; Zhang, X.; Groopman, J. E. Activation of Vascular Endothelial Growth Factor Receptor-3 and Its Downstream Signaling Promote Cell Survival under Oxidative Stress. *J. Biol. Chem.* **2004**, *279*, 27088−27097.

DOI: 10.1021/acsami.5b00130
ACS Appl. Mater. Interfaces 2015, 7, 5944−5949